Liquid Crystals

ISSN: (Print) (Online) Journal homepage: https://www.tandfonline.com/loi/tlct20

Precision adiabatic scanning calorimetry of a nematic – ferroelectric nematic phase transition

Jan Thoen, Eva Korblova, David M. Walba, Noel A. Clark & Christ Glorieux

To cite this article: Jan Thoen, Eva Korblova, David M. Walba, Noel A. Clark & Christ Glorieux (2021): Precision adiabatic scanning calorimetry of a nematic – ferroelectric nematic phase transition, Liquid Crystals, DOI: 10.1080/02678292.2021.2007550

To link to this article: https://doi.org/10.1080/02678292.2021.2007550

LIQUID CRYSTALS
https://doi.org/10.1080/02678292.2021.2007550

Taylor & Francis
Taylor & Francis Group

Precision adiabatic scanning calorimetry of a nematic – ferroelectric nematic phase transition

Jan Thoen[a], Eva Korblova[b], David M. Walba[b], Noel A. Clark[c] and Christ Glorieux[a]

[a]Laboratory for Soft Matter and Biophysics, Department of Physics and Astronomy, KU Leuven, Leuven, Belgium; [b]Department of Chemistry and Soft Materials Research Center, University of Colorado, Boulder, CO, USA; [c]Department of Physics and Soft Materials Research Center, University of Colorado, Boulder, CO, USA

ABSTRACT

In high-resolution adiabatic scanning calorimetry (ASC) experiments, data for the temperature dependence of the specific enthalpy, $h(T)$, and of the specific heat capacity, $c_p(T)$, are simultaneously obtained, from which the order of the phase transition and critical behaviour can be evaluated. ASC was applied to study the nematic to ferroelectric nematic phase transition (N–N_F) in the liquid crystal molecule 4-[(4-nitrophenoxy)carbonyl]phenyl 2,4-dimethoxybenzoate (RM734). The N–N_F was found to be very weakly first order with a latent heat $\Delta h = 0.115 \pm 0.005$ J/g. The pretransitional specific heat capacity behaviour is substantially larger in the high-temperature N phase than in the low-temperature N_F phase. In both phases the power-law analysis of $c_p(T)$ resulted in a critical exponent $\alpha = 0.50 \pm 0.05$ and amplitude ratio $A_{NF}/A_N = 0.42 \pm 0.03$. The very small latent heat and the value of α indicate that the N–N_F transition is close to a tricritical point. This is confirmed by a value of the order parameter exponent $\beta \approx 0.25$, recently obtained from electric polarisation measurements. Invoking two-scale-factor universality, it follows from the low value of A_{NF}/A_N ratio that the size of the critical fluctuations is much larger in the N_F phase than in the N phase.

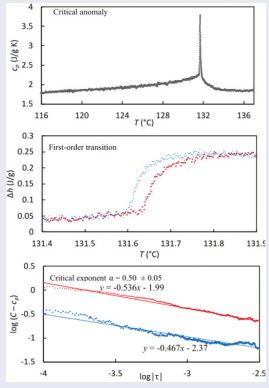

ARTICLE HISTORY
Received 17 October 2021
Accepted 14 November 2021

KEYWORDS
Heat capacity; enthalpy; ferroelectric nematic; tricritical point

1. Introduction

The rod-shaped mesogenic molecule 4-[(4-nitrophenoxy) carbonyl]phenyl 2,4-dimethoxybenzoate (RM734) has recently been shown to exhibit a thermotropic phase transition between a uniaxial dielectric nematic phase (N) and a lower temperature ferroelectric nematic phase, the N_F phase, in the vicinity of T = 133°C [1]. The N_F phase exhibits, in the absence of applied field, a permanent electric polarisation density, manifested as a spontaneously broken symmetry in distinct domains of opposite polar orientation [2]. Polarisation reversal is mediated by field-induced domain wall movement, making this phase ferroelectric, a three–dimensional uniaxial nematic having a spontaneous, reorientable, polarisation density $\boldsymbol{P}(r)$, locally colinear with the nematic director field, $\boldsymbol{n}(r)$, giving the local average molecular long axis. This polarisation density increases monotonically upon cooling in the N_F phase from a small value near the transition to saturate at a low-temperature value of ~6 μC/cm^2, with no other significant birefringence or internal structural changes. This polarisation is the largest ever measured for a fluid or glassy material and is close to the average value obtained by assuming perfect, polar alignment of molecular long axes. The ultimate polarised state at low temperature exhibits little response to large applied fields tending to increase P (i.e. $\boldsymbol{E}$ parallel to $\boldsymbol{P}$).

CONTACT Jan Thoen jan.thoen@kuleuven.be

These conditions indicate that the ground state of the N_F phase has, aside from fluctuations, uniform $\boldsymbol{P}$ and that it is a proper ferroelectric phase, where P is the principal order parameter. Under this condition, the N–N_F transition can be viewed as Ising-like, with the N phase being a collection of molecules with long axes on average colinear with $\boldsymbol{n}$ but with disordered polar directions ($p_i = 0$) , and the N_F phase also having long axes on average parallel to $\boldsymbol{n}$, with polar order $N(p_i) = P$. Atomistic molecular dynamic simulations of several hundreds of molecules reveal short-range interactions and correlations, including polar end-to-end association, that favour ferroelectric ordering. With these interactions this transition would be predicted to be second order with 3D critical exponents of the Ising universality class [3].

However, low-resolution differential scanning calorimetry (DSC) indicates that the transition is weakly first order, and the Mertelj group [4,5] has observed spectacular paraelectric pretransitional effects upon cooling towards the transition in the N phase, including the softening of the splay elastic constant, K_s, and a divergence of the dielectric anisotropy $\Delta\varepsilon$, that are distinctly mean-field like. The softening of K_s is due to the flexoelectric coupling between polarisation fluctuations and director splay as the transition is approached from above, observations which they have interpreted using a Landau–de Gennes model [4–6]. The free energy of Ref [5], $f = ½\,[\tau(T)(1 + \xi(T)^2 q^2)\delta P_z(q)^2 + K_s\, q_y{}^2 \delta n_y(q_y)^2] + \gamma\, q_y \delta n_y(q_y)\, \delta P_z(q_y)$, where $\xi(T)^2 = b/\tau(T)$, $\tau(T) \propto (T\text{-}T_c)/T_c$, and $\boldsymbol{q} = \boldsymbol{q}_z + \boldsymbol{q}_y$, includes OrnsteinZernicke polarisation fluctuations about $q = 0$, originating from short-range polar interactions, and the flexoelectric coupling of P_z to director splay. This model successfully describes a mean field-like behaviour of $K_s(\tau)$ and $\Delta\varepsilon(\tau)$. This free energy is consistent with the N_F phase having uniform $\boldsymbol{P}$, with a weak tendency for splay that is suppressed by polarisation space charge effects.

An additional pretransitional effect not yet adequately characterised or described is the striking anisotropy of the pretransitional and coarsening correlations in the fluctuations of $\boldsymbol{P}$ through the transition, with the domains becoming increasingly extended along $\boldsymbol{z}$, until they end up as polar regions separated by pure polarisation reversal walls running largely parallel to $\boldsymbol{z}$. [Ref. [2], Figs. S8,9)]. Given the significant anisotropies introduced into the N_F phase by space charge effects, it is natural to consider that the polarisation charge energy U_P associated with electric dipole–dipole interactions may also affect the phase transition and pretransitional fluctuations. The resulting interaction energy combines short-ranged ferroelectric and long-ranged dipole-dipole forces.

The short-range ordering effect of electrostatic interactions on the transition can be understood directly by considering a single dipolar RM734 molecule in the N_F phase to be at the origin of a coordinate system surrounded by its neighbours. Referring to Figs. 7 and S10–13 of [2], neighbouring molecules are positionally correlated, so, although the macroscopic electric field $\boldsymbol{E} = 0$, correlations lead to local electric fields that stabilise polar ordering (the nearest neighbour Ising field). The RM734 molecule has parallel longitudinal dipoles at its two ends, which find themselves in inhomogeneous electric fields from their head-to-tail-associating neighbours, fields that stretch the molecule out along its polar axis, orientationally confining it in polar fashion.

The critical behaviour of such systems has been studied extensively in an effort to understand certain magnetic materials that have short-range ferromagnetic exchange forces, but where the long-range dipolar interactions are also important [7,8]. In these systems, short-ranged interactions are included in a model Hamiltonian as nearest-neighbour Ising or Heisenberg-like, and the long-ranged dipolar interactions are calculated explicitly. Renormalisation group analysis shows that the long-range interactions make the magnetic correlations dipolar-anisotropic near the transition in the high-temperature phase [9,10], extending them along $\boldsymbol{z}$ by strongly suppressing longitudinal charge density ($\partial Pz/\partial z$) fluctuations [7,8]. Specifically, starting with the free energy expression Equation (1) from Ref. [5] and adding the dipole–dipole interaction term U_P from above, the structure factor for fluctuations in P_z becomes

$$\langle P_z(q) P_z(q)* \rangle = k_B T \chi(q)$$

where

$\chi(q) = [\tau(T)(1 + \xi(T)^2 q^2) + (2\pi/\varepsilon)(q_z/q)^2]^{-1}$.

The dipole–dipole (third) term produces extended correlations that grow as $\xi(\tau)$ along x and y but as $\xi(\tau)^2$ along z [8], suppressing $\chi(\boldsymbol{q})$ for finite q_z as is observed qualitatively from the image sequences of the textures upon passing through the phase transition, and from their optical Fourier transforms [Ref. [2], Figs. S8,9)]. Because of this anisotropy, the correlation volume in this model grows in 3D as $V \sim (\tau)^4$ rather than the isotropic $V \sim \xi(\tau)^3$, reducing the upper marginal dimensionality of the transition to 3D, making the transition mean-field-like with logarithmic corrections, rather than fluctuation-dominated with 3D Ising universality [11].

From the above overview of the present understanding and cited references, it is clear that theoretical modelling has led to the better insight in several aspects of

experimental results and observations of RM734. However, other aspects and possible theoretical propositions require further experimental testing, as, for example, the order of the nematic to ferroelectric nematic ($N–N_F$) transition and the nature of the pretransitional critical behaviour. Although DSC measurements [1,2,12] have indicated a first-order character for the $N–N_F$ transition, some caution is required because of the inherent difficulty of DSC with the distinction between real latent heats and pretransitional fluctuation-induced enthalpy increases, as historically well documented, in particular for the nematic to smectic A transition [13–16]. In an effort to contribute to further understanding of the $N–N_F$ transition, we report high-resolution specific heat capacity and specific enthalpy results by high-resolution adiabatic scanning calorimetry (ASC).

2. Experimental

2.1. Adiabatic scanning calorimetry

2.1.1. Adiabatic scanning calorimetry: operational principle

ASC was developed to obtain simultaneously and continuously the temperature evolution of the heat capacity C_p and the enthalpy H of a sample under investigation [15–20]. The basic concept of ASC is in applying a constant heating or cooling power to a sample holder containing the sample. In an ASC the sample holder is placed inside a surrounding adiabatic shield. In a heating run the heat exchange between shield and sample holder is cancelled by keeping the temperature difference zero at all times. In a cooling run the heat exchange is controlled and monitored. During a run the sample temperature $T(t)$ is recorded as a function of time t. Together with the applied power P this directly results in the enthalpy curve

$$H(T) - H(T_0) = \int_{t_0}^{t(T)} P dt = P[t(T) - t_0(T_0)], \quad (1)$$

where $H(T_0)$ is the enthalpy of the system at temperature T_0 at the starting time t_0 of the run. The heat capacity $C_p(T)$ is easily calculated via the ratio of the know constant power P and the changing temperature rate $\dot{T} = dT/dt$,

$$C_p = \frac{P}{\dot{T}}. \quad (2)$$

The specific values of the heat capacity c_p and of the enthalpy h are obtained by using the sample mass and the calibrated background values of the empty calorimeter and of the used sample cell. It should be noted that keeping P constant in Equation (2) is completely opposite to the operation of a DSC where one imposes a constant rate $\dot{T}$ on a sample and on a reference and measures the difference in heat flux, $\Delta P(t)$, between the sample and the reference.

2.1.2. Peltier-element-based adiabatic scanning calorimeter (pASC)

An essential requirement for a high-resolution adiabatic scanning calorimeter operating in the heating mode is the equality (mK or better) of the temperatures of the adiabatic shield and of the sample (holder) in weak thermal contact with this surrounding adiabatic shield. For cooling mode operations, a constant preset temperature difference between the sample and the shield has to be maintained within the same temperature stability limits. The 'classical' ASC implementations used elaborate construction and calibration procedures to achieve these conditions [15–20]. All this made these ASC instruments complicated. In the present type of ASC, used for the results presented here, these problems are completely eliminated by inserting a very sensitive (of the order of 10 mV K^{-1}) semiconductor-materials-based Peltier element (PE) as temperature difference detector between the sample and the shield. The μK sensitivity of the PE for temperature differences allows, in combination with a proper servo-system, to maintain almost perfect equality of the sample and shield temperatures in the heating mode. For the cooling mode, a preset temperature difference between sample and shield can be kept constant with equal resolution. Details on the construction of the pASC implementation of the ASC concept can be found elsewhere [21–25]. With the pASC used for the present investigation, the uncertainty on the absolute values of specific heat capacity and enthalpy is about 2%, while the resolution in these quantities and in the measured temperatures is much higher.

2.2. Material and sample preparation

Calorimetric measurements by pASC are reported for the calamitic compound 4-[(4-nitrophenoxy)carbonyl] phenyl 2,4-dimethoxybenzoate (RM734) around the nematic to ferroelectric nematic phase transition [1,2]. The compound was synthesised at the Soft Materials Research Center of the University of Colorado [Ref. [2], Figure S1]. The compound was used as received at the Laboratory for Soft Matter and Biophysics at KU Leuven. An amount of 60.1 mg of sample was transferred in a stainless steel sample holder (Mettler Toledo 120 μl medium pressure DSC crucibles) and hermetically sealed.

3. Measurements

After the sample cell was mounted in the calorimeter, the calorimeter was heated to 110°C where a heating run at an *average* heating rate of 0.048 K/min was started through the melting transition to 146°C. From that temperature a cooling run at an average cooling rate of 0.025 K/min was carried out. Subsequently, a heating run at an average rate of 0.041 K/min was done through the N–N_F transition (around 133°C), followed by a cooling run through this transition. Several other heating and cooling runs at different (lower) heating or cooling settings were done for consistency tests. At all times the sample remained in the subcooled phase and no rate dependence was observed and results were fully consistent. After this set of measurements the sample cell was taken out of the calorimeter and heated up to 200°C well into the isotropic phase, cooled to room temperature and placed back in the pASC. Part of the initial set of runs was repeated. No changes in the results were seen. Although results were obtained for the melting transition, here we will only consider the results for the nematic-to-ferroelectric nematic transition.

4. Results

In Figure 1(a) an overview of the specific heat capacity $c_p(T)$ is given for the temperature range between 116°C and 137°C from a heating run. The sharpness of the peak and the clear slope discontinuity on the low-temperature side suggests a first-order transition (see further). There is, however, in particular in the high-temperature phase, nonlinear pretransitional specific heat capacity variation. In a cooling run similar results were measured but with a small shift to a lower peak temperature value (see further). In Figure 1(b) a blow-up of $c_p(T)$ from a cooling run is given for a 1 K temperature range. In Figure 2 the temperature dependence of the specific enthalpy is given over the 130–133°C temperature range. At the transition temperature there is in the almost linear temperature dependence a very small upward increase, indicating a very small transition energy.

In order to have a better view on the transition one can subtract a linear temperature-dependent background from the data displayed in Figure2. This corresponds to subtraction of a constant specific heat capacity value from the data in Figure 1. Indeed, in a sample with a constant

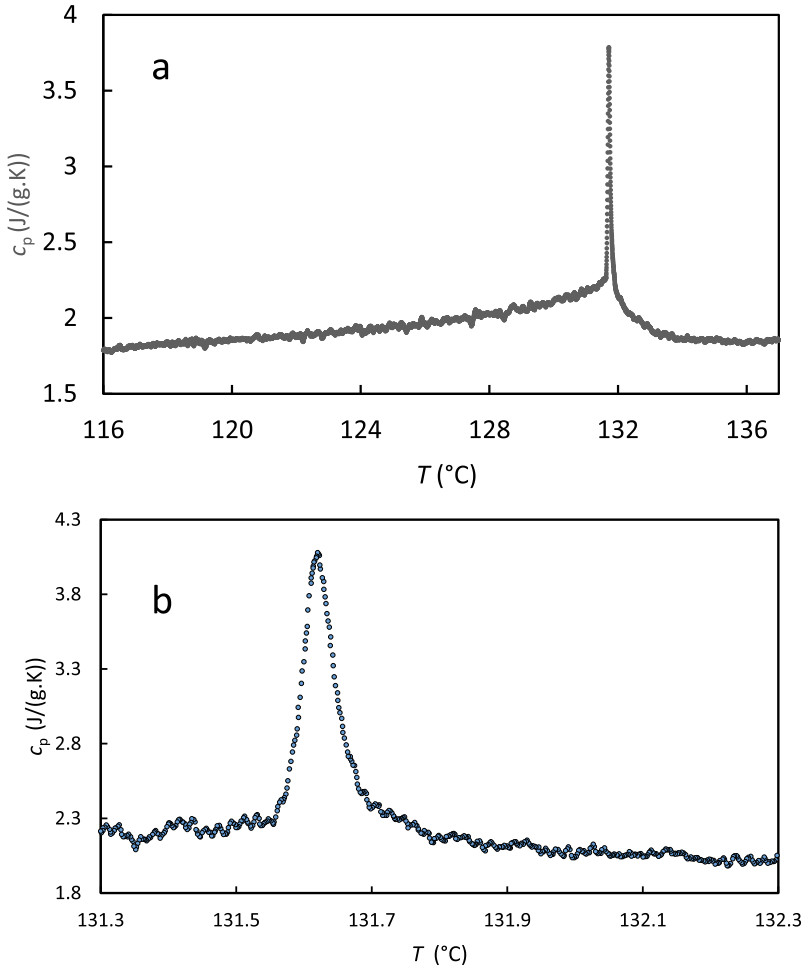

Figure 1. (Colour online). (a) Temperature dependence of the specific heat capacity across the transition from the ferroelectric nematic N_F phase to the nematic N phase of RM734 from a heating run. (b) Detail of the temperature dependence of the specific heat capacity in a temperature range of 1 K over the transition from the ferroelectric nematic N_F phase to the nematic N phase of RM734 from a cooling run.

heat capacity the enthalpy increases linearly. This is done in an intermediate step in the inset of Figure 2 where now the enthalpy increase is much better visible. This procedure has been extended in Figure 3 to a very narrow temperature range of 500 mK covering the transition. From these heating run data (see Figure 3) it is possible to identify a small two-phase region (with linear enthalpy dependence) between 131.635°C and 131.669°C, and thus with a width of 34 mK. The latent heat associated with the (very) weakly first-order transition is 0.115 ± 0.005 J/g.

In Figure 3 a comparison is also made between the heating run results and results of a cooling run over the same temperature range. The data are very similar, but shifted down for the cooling run by 27 mK. This small undercooling is consistent with the (weakly) first-order character of the transition. The latent heat value of 0.115 J/g is substantially lower than the transition heats obtained by DSC, 0.47 J/g in refs [1.12] and 1.04 J/g in ref. [2]. This is not a surprise because DSC cannot make a distinction between true latent heats and pretransitional

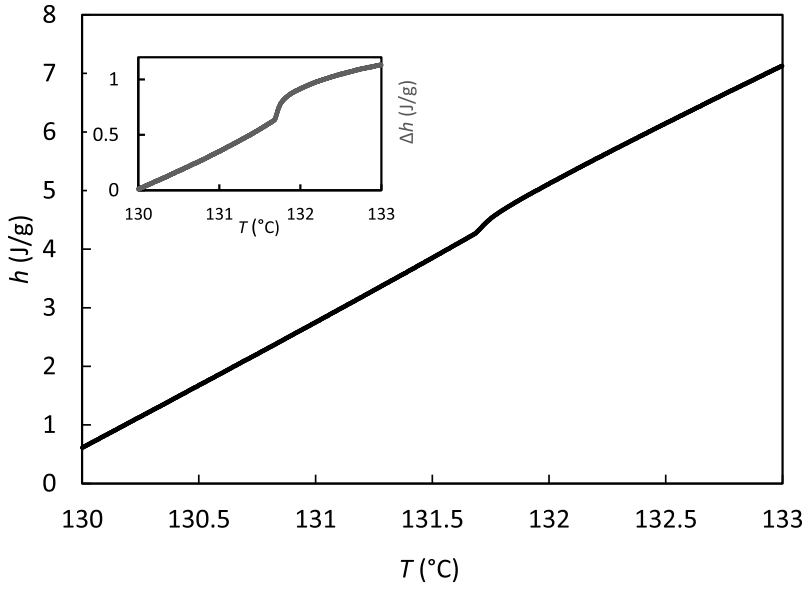

Figure 2. (Colour online). Temperature dependence of the specific enthalpy across the transition from the ferroelectric nematic N_F phase to the nematic N phase in RM734. Inset: temperature dependence of the specific enthalpy after subtraction (for display reasons) of a linear temperature-dependent background, $1.5(T - T_{ref})$ (J/g), with T_{ref} an arbitrary reference temperature.

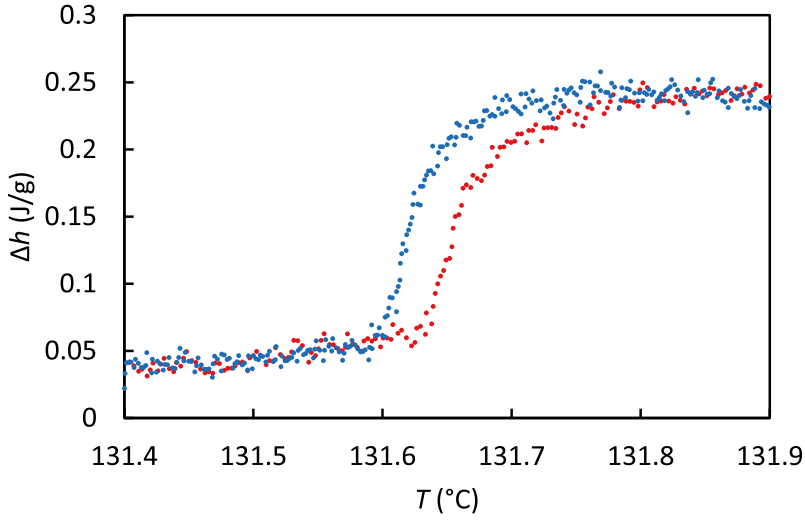

Figure 3. (Colour online). Temperature dependence of the specific enthalpy near the ferroelectric nematic N_F to nematic N transition of RM734 over a 500 mK temperature range. The red dots (to the right) for a heating run correspond with the data of Figure 2. The blue dots (to the left) are from a cooling run over the same temperature range. For display reasons a linear temperature dependent background has been subtracted in both cases.

(fluctuations induced) enthalpy (heat capacity) changes [14–16] because, in DSC, the total enthalpy change is deduced from integration of a heat flux peak (often scanning rate broadened) between (chosen) onset and endset temperatures. This is in particular a problem when true latent heats are comparable or smaller than pretransitional effects. The problem is smaller in DSC for large latent heats, as, for example, for melting transitions.

5. Data analysis

5.1. Background specific heat capacity

From Figure 1 it can be observed that in the low-temperature range there is an almost linear temperature dependence of the specific heat capacity and only near the transition a relatively small enhancement is observed. On the high-temperature side pretransitional variation is substantially larger. It also seems that there, in the N phase, the regular background behaviour drops down to a value smaller than in the N_F phase. This is better seen in Figure 4(a) where a linear background (from a fit of the c_p between 117 and 125°C) has been subtracted from c_p. A clearly lower background is present in the N phase. This is further illustrated in Figure 4(b), where the data of Figure 4 (a) are displayed as a function of the absolute temperature difference $|T - T_{tr}|$ from the transition temperature T_{tr}. From this figure it is obvious that the background c_p value in the N phase is lower than in the N_F phase, the difference being 0.27 J/(gK). From Figure 4(a, b) it is also clear that the pretransitional specific heat capacity increase in the N phase is substantially larger than in the N_F phase.

5.2. Specific heat capacity anomaly

Second-order (continuous) phase transitions are characterised by fluctuations, which, for a properly defined order parameter, diverge in size to infinity. This size divergence can be described by a power law, with a characteristic critical exponent depending on the universality class of the phase transition [26]. The limiting behaviour of the specific heat capacity at a second-order phase transition can also be described by means of a power law of the form

$$c_p = A|\tau|^{-\alpha} + B, \tag{3}$$

with $\tau = (T - T_c)/T_c$. The parameter A is the critical amplitude, α is the critical exponent, T_c is the critical temperature (T and T_c in kelvin) and B is the background term. The different coefficients in Equation (3) must be derived from (non-linear) least-squares fitting of experimental data. However, the fact that ASC scans result directly in enthalpy $h(T)$ data (see Equation (1)) allows substantial simplification. One can define the following quantity

$$C = \frac{h - h_c}{T - T_c}, \tag{4}$$

which corresponds to the slope of the chord connecting $h(T)$ at T, with h_c at T_c. It can easily be shown that C has a power-law behaviour of the form [15,18,20]

$$C = \frac{A}{1-\alpha}|\tau|^{-\alpha} + B. \tag{5}$$

Both c_p and C have the same critical exponent, and either Equation (3) or (5) can be used in fitting data to arrive at important values for the critical exponent α and amplitude A. However, by considering the difference $(C - c_p)$, above or below T_c, the (unimportant) background term B drops out, resulting in

$$C - c_p = \frac{\alpha A}{1-\alpha}|\tau|^{-a}. \tag{6}$$

Taking the logarithm on both sides of Equation (6) gives

$$\log(C - c_p) = \log\left(\frac{\alpha A}{1-\alpha}\right) - \alpha\log|\tau|. \tag{7}$$

As a result, one obtains (sufficiently close to the critical point) a straight line with a negative slope immediately giving the critical exponent α.

This procedure is strictly only applicable to second-order transitions, but for weakly first-order transitions it can be used for separate analysis of the data below and above the transition by allowing T_c and h_c in Equation (4) to be adjustable parameters in fitting that can be different for data below and above the transition. This is analogous to the upper stability limit of the nematic phase and the lower stability limit of the isotropic phase for the weakly first-order nematic–isotropic transition [18,27]. We have applied this approach to the present phase transition data of and h (see Figures 1 and 2), excluding the data in the two-phase region.

In Figure 5, data for the two quantities C and c_p are given for this N–N_F transition. The corresponding logarithmic plot (see Equation (7)) is given in Figure 6. It can be concluded that, within experimental resolution, a negative slope of −0.50 ± 0.05 is consistent with the data. Thus, according to Equation (7) this results in a critical exponent $\alpha = 0.50 \pm 0.05$. In Figure 6, it can also be seen that $(C - c_p)$ above the transition (in the normal) N phase is much larger than in the N_F phase below the transition. From Equation (6) it immediately follows that the critical amplitude in the ferroelectric nematic

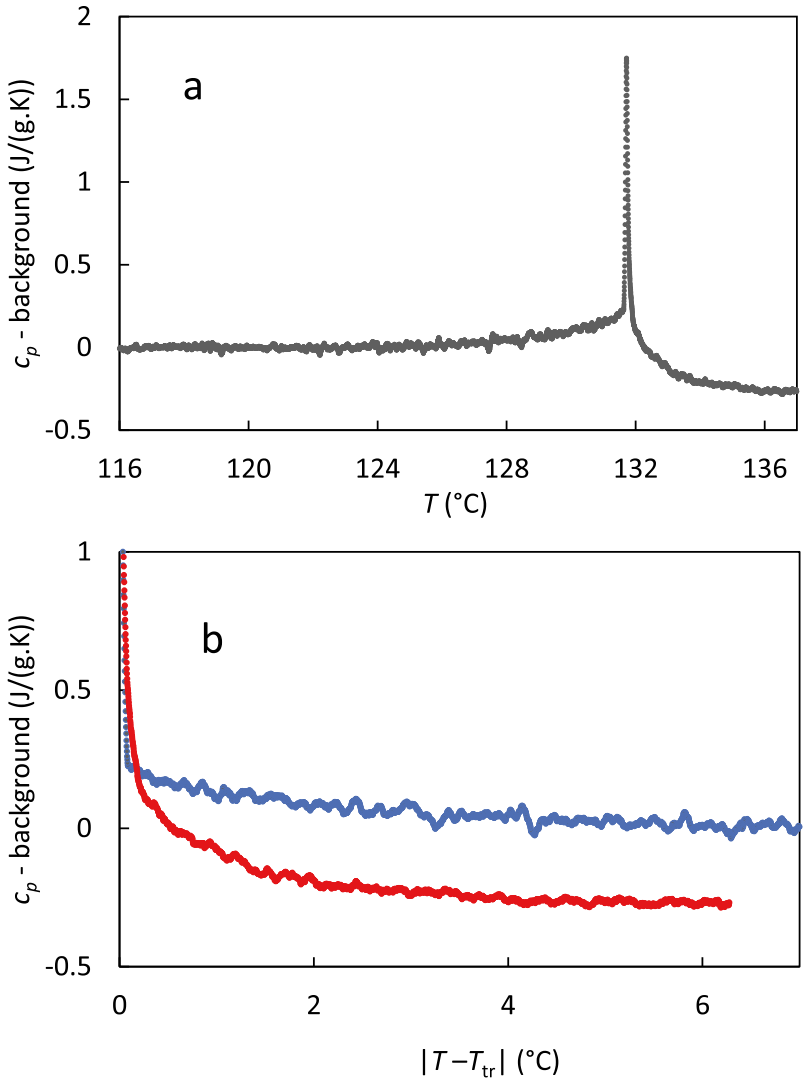

Figure 4. (Colour online). (a) Temperature dependence of the specific heat capacity over the ferroelectric nematic N_F to nematic N transition of RM734 after subtraction of a linear background obtained from a linear fit of the data between 117 and 125°C. (b) The specific heat capacity as a function $|T - T_{tr}|$ (with T_{tr} the transition temperature) for the N_F (upper blue data) and N (lower red data) phase after subtraction of a linear background obtained from a linear fit of the data between 117°C and 125°C.

phase, A_{FN}, must be substantially smaller than the critical amplitude in the nematic phase, A_N. A rough estimate gives for the ratio $A_N/A_{FN} = 2.4 \pm 0.2$.

6. Discussion

As described in the introduction, depending on the molecular interactions considered, different possibilities arise for the N–N_F phase transitional behaviour of the liquid crystal RM734. Considering the molecular interactions and correlations (including end-to-end association) at short range predicts the transition to be a second-order one belonging to the 3D Ising universality class [3]. However, the experimental observed pretransitional softening of the splay elastic constant and the divergence of the dielectric anisotropy showed mean-field-like behaviour that could be interpreted using a Landau–de Gennes model [4–6]. Also the DSC indications of a first-order character of the transition can possibly be accounted for by the same Landau–de Gennes model by adding higher-order terms. From the analogy with certain magnetic materials, where, in addition to short-range ferromagnetic exchange forces, also long-range dipolar interactions are important [7,8], a 3D upper marginal dimensionality of the transition is obtained, making the transition mean-field-like with logarithmic corrections [11].

Since in high-resolution ASC experiments direct experimental data for the temperature dependence of the specific enthalpy, $h(T)$, and of the specific heat capacity, $c_p(T)$, are obtained, the order of the phase transition as well as the fluctuations-induced critical

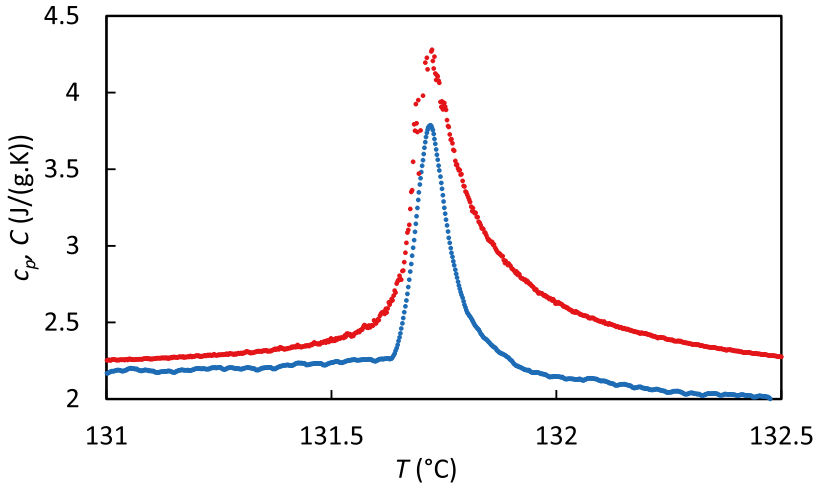

Figure 5. (Colour online). Adiabatic scanning calorimetry results above and below the N_F–N transition of RM734. The lower (blue) curve are the specific heat capacity c_p values and the upper (red) curve are the quantity C values defined in Equation (4).

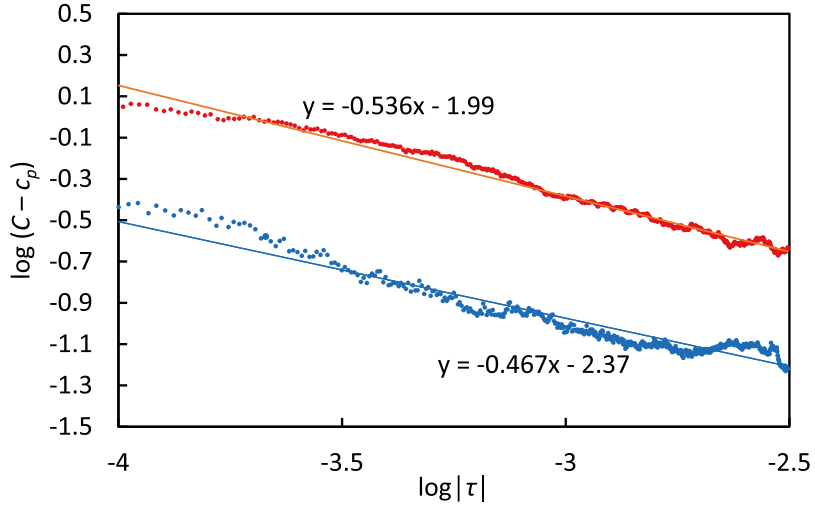

Figure 6. (Colour online) Adiabatic scanning calorimetry results for the N_F–N transition of RM734. Double logarithmic plot of the difference ($C - c_p$) expressed in J/(gK) as a function of the reduced temperature difference τ. The lower blue points are for $T < T_c$ and the upper red ones for $T > T_c$. The slopes (−0.536 and −0.467) of the linear trend lines are consistent with a critical exponent $\alpha = 0.50 \pm 0.05$.

behaviour can be evaluated. From the direct $h(T)$ discussed in Section 4 and displayed in Figure 3, it is clear that the N–N_F transition in RM734 is, although very weakly, first order. The obtained value for the latent heat $\Delta h = 0.115 \pm 0.005$ J/g is a factor 5–10 smaller than the DSC values [1,2,12], which most likely contain also pretransitional fluctuations-induced contributions.

The critical behaviour of several physical parameters near phase transitions is described by power laws with critical exponents and by amplitude ratios depending on the spatial dimension (D) and the type and universality class of the transition. Several models, for example, those with vector order parameters of dimension $n = 1$ (Ising model), $n = 2$ (XY model) and $n = 3$ (Heisenberg model), have resulted in high-quality numerical predictions for many critical exponents. The most relevant critical exponents are α for the specific heat capacity, β for the order parameter, γ for the susceptibility and ν for the correlation length. For the $D = 3$ case relevant sets of exponents are Ising (n = 1) $\alpha = 0.110$, $\beta = 0.325$, $\gamma = 1.241$, $\nu = 0.63$; tricritical $\alpha = 0.5$, $\beta = 0.25$, $\gamma = 1$, $\nu = 0.5$; mean field $\alpha = 0$, $\beta = 0.5$, $\gamma = 1$, $\nu = 0.5$ [28–30]. From these values it should be clear that in particular differences for α, and to a lesser extent also for β, are quite large.

The ASC data for the temperature dependence of the specific heat capacity $c_p(T)$ near the transition allows one to derive information on the critical exponent α and the

critical amplitude ratio A_{NF}/A_N These $c_p(T)$ data are displayed in Figure 1 and analysed in detail in Section 5. However, before discussing the results of the analysis for these parameters, some unusual features of the $c_p(T)$ data have to be considered. From the analysis in Section 5.1 it was concluded that in the N phase the regular $c_p(T)$ background drops down to a value smaller than in the N_F phase. This is illustrated in Figure 4(a, b). The difference is estimated to be 0.27 J/(gK). In Figure 4(a, b) it can also be observed that the specific heat capacity increase in the N phase is substantially larger than in the N_F phase. Thus, in the high-temperature nematic phase the pretansitional (fluctuations-induced) effects are much larger than in the ferroelectric nematic phase. Larger pretransitional effects in the high-temperature phase than in the low-temperature (more ordered) phase are not very common, but not unique. For example, Garland and Co-workers [31] observed a large inverted-Landau behaviour in the high-temperature Sm $\tilde{C}$ phase at a SmC-Sm $\tilde{C}$ transition, where apparently polarisation order plays a role.

In Section 5.2 it was demonstrated how the ASC $c_p(T)$ and $h(T)$ data can be combined in a unique way to arrive at information about the critical exponent α and the critical amplitude ratio A_{NF}/A_N by eliminating the otherwise difficult to evaluate background contributions. This procedure leads to the new quantity $(C–c_p)$ displayed versus the reduced temperature difference $|\tau|$ (of Equation 3) in a double logarithmic plot which leads to $\alpha = 0.50 \pm 0.05$ and $A_{NF}/A_N = 0.42 \pm 0.03$. The value of α is consistent with the value for a (nearby) tricritical point, located at the crossover from first order to second order along a phase transition line that could be established by an external driving field (e.g. electric, magnetic, pressure, mole fraction in mixtures, etc.). The tricritical character of the N–N_F transition in RM734 has very recently been confirmed by measurements of the temperature dependence of the order parameter (electric polarisation) in the N_F phase, growing with decreasing temperature as a power law $P \propto (T_c - T)^{\beta}$, with a critical exponent $\beta \approx 0.25$ which is, indeed, the tricritical value [32].

Although the critical amplitude ratio, here for the specific heat $r = A^-/A^+ \equiv A_{FN}/A_N$, is quite an important result for many phase transitions, this is less the case for the tricritical case since it is known that tricritical ratios determined over accessible $|\tau|$ ranges are not universal. For an exactly solvable spherical model ($n = \infty$) they are nonuniversal but functions of a single variable $z = (a/R_0)^3$, where a is the lattice spacing and R_0 the range of interactions [33,34]. Applying the relation $r = (1 - z^2)^{1/2}/z$ (assuming logarithmic corrections can be ignored for finite n [35]) obtained by Fisher and Sarbach [33,34], results for our value of $A_{FN}/A_N = 0.42$ in $z = 0.92$. The amplitude ratio $r = \infty$ for the Landau tricritical point is recovered for $z = 0$. For $r = 1$ a value of $z = 0.707$ is obtained. This theory was used to explain the tricritical ratios behaviour for ^{3}He–^{4}He mixtures ($z = 0.12$) and for the metamagnet dysprosium aluminium garnet ($z = 0.21$). Applying this approach to liquid crystal nematic–smectic-A tricritical points in binary mixtures by Stine and Garland [36] resulted in $z = 0.71$ for polar compounds and in $z = 0.53$ for non-polar ones. From a similar analysis of heat capacity data near a smectic-A–smectic-C tricritical point in a racemic liquid crystal mixture, Ema et al. [37] yielded a value $z = 0.11$. If this approach holds also in the case of the N–N_F transition in RM934, the quite large value of $z = 0.92$ indicates that the transition is quite far from the Landau theory limit.

In addition to the presently available experimental values $\alpha \approx 0.50$ and $\beta \approx 0.25$, indicating tricritical behaviour, further experimental results on the temperature dependence of the correlation length (with critical exponent ν) in the two phases (e.g. from x-ray scattering) would be very important. In the framework of two-scale-factor universality [38], the quite small value $A_{NF}/A_N = 0.42$ indicates that the size of the critical fluctuations in the N_F phase should be substantially larger than in the N phase. Indeed, in two-scale universality it is stated that the specific heat amplitudes A_{NF} and A_N are *inversely* proportional to the third power of the corresponding amplitudes ξ_0 in the power laws for the correlation lengths of the critical fluctuations.

Disclosure statement

No potential conflict of interest was reported by the author(s).

Funding

This work was supported by NSF Condensed Matter Physics Grants DMR 1710711 and DMR 2005170, and by Materials Research Science and Engineering Center (MRSEC) Grant DMR 1420736.

References

[1] Mandle RJ, Cowling SJ, Goodby JW. Rational design of rod-like liquid crystals exhibiting two nematic phases. Chem Eur J. 2017;23:14554–14562.
[2] Chen X, Korblova E, Dong D, et al. First-principles experimental demonstration of ferroelectricity in a thermotropic nematic liquid crystal: polar domains and striking electro-optics. PNAS. 2020;117:14021–14031.
[3] Als-Nielsen J, Birgeneau RJ. Mean field theory, the Ginzburg criterion, and marginal dimensionality of phase transitions. Am J Phys. 1977;45:554–560.

[4] Mertelj A, Cmok L, Sebastián N, et al. Splay nematic phase. Phys Rev X. 2018;8:041025.
[5] Sebastián N, Cmok L, Mandle RJ, et al. Ferroelectric-ferroelastic phase transition in a nematic liquid crystal. Phys Rev Lett. 2020;124:037801.
[6] Copic M, Mertelj A. Q-tensor model of twist-Bend and splay nematic phases. Available from: https://arxiv.org/pdf/1910.01424.pdf
[7] Kotzler J. Critical phenomena in dipolar magnets. J Magn Magn Mater. 1986;54-57:649–654.
[8] Als-Nielsen J. Experimental test of renormalization group theory on the uniaxial, dipolar coupled, ferromagnet $LiTbF_4$. Phys Rev Lett. 1976;37:1161–1164.
[9] Aharony A, Fisher ME. Critical behavior of magnets with dipolar interactions. 1. Renormalization group near 4 dimensions. Phys Rev B. 1973;8:3323–3341.
[10] Aharony A. Critical behavior of magnets with dipolar interactions. 5. Uniaxial magnets in d-dimensions. Phys Rev B. 1973;8:3363–3370.
[11] Ahlers G, Kornblit A, Guggenheim HJ. Logarithmic corrections to the Landau specific heat near the Curie temperature of the dipolar Ising ferromagnet LiTbF4. Phys Rev Lett. 1975;34:1227–1230.
[12] Connor RLM, Mandle RJ. Chemically induced splay nematic phase with micron scale periodicity. Soft Matter. 2020;16:324–329.
[13] Kasting GB, Lushington KJ, Garland CW. Critical heat capacity near the nematic-smectic-A transition in octyloxycyanobiphenyl in the rang 1-2000 bar. Phys Rev B. 1980;22:321–331.
[14] Kasting GB, Garland CW, Lushington KJ. Critical heat capacity of octylcyanobiphenyl (8CB) near the nematic-smectic-A transition. J Phys. 1980;41:879–884.
[15] Thoen J, Marynissen H, Van Dael W. Temperature dependence of enthalpy and the heat capacity of the liquid crystal octylcyanobiphenyl (8CB). Phys Rev A. 1982;26:2886–2905.
[16] Thoen J. Calorimetric studies of liquid crystal phase transitions: steady state adiabatic techniques. In: Martellucci S, Chester AN, editors. Phase Transitions in Liquid Crystals. New York (NY): Plenum Press; 1992. p. 155–173.
[17] Thoen J, Bloemen E, Marynissen H, et al. High-resolution calorimetric investigations of phase transitions in liquids. In: Sengers JV, editor. Proceedings of the 8th Symposium on Thermophysical Properties; 1981 June 15-18; Gaithersburg (MD); New York(NY): Am Soc Mech Eng; 1982. p. 422–428.
[18] Thoen J. Thermal investigations of phase transitions in thermotropic liquid crystals. Int J Mod Phys B. 1995;9:2157–2218.
[19] Thoen J. High resolution adiabatic scanning calorimetry and heat capacities. In: Wilhelm E, Letcher T, editors. Heat capacities: liquids, solutions and vapours. Cambridge (UK): RSC Publishing; 2010. p. 287–328.
[20] Thoen J, Cordoyiannis G, Glorieux C. Investigation of phase transitions in liquid crystals by means of adiabatic scanning calorimetry. Liq Cryst. 2009;36:669–684.
[21] Thoen J, Leys J, Glorieux C. Adiabatic scanning calorimeter. European Patent EP 2 91328 B1 (Sept 02, 2015). US Patent US 9.310.263 B2. 2016 Apr 12.
[22] Leys J, Losada-Pérez P, Glorieux C, et al. Application of a novel type of adiabatic scanning calorimeter for high-resolution thermal data near the melting point of gallium. J Therm Anal Calorim. 2014;117:173–187.
[23] Thoen J. Enthalpy measurements of condensed matter by Peltier-element-based adiabatic scanning calorimetry (pASC). In: Wilhelm E, Letcher T, editors. Enthalpy and internal energy: liquids, solutions and vapours. Croydon (UK): RSC; 2018. p. 77–95.
[24] Thoen J, Cordoyiannis G, Losada-Pérez P, et al. High-resolution investigation by Peltier-element-based adiabatic scanning calorimetry of binary liquid crystal mixtures with enhanced nematic ranges. J Mol Liq. 2021;340:117204.
[25] Thoen J, Cordoyiannis G, Glorieux C. Adiabatic scanning calorimetry investigation of the melting and order–disorder phase transitions in the linear alkanes heptadecane and nonadecane and some of their binary mixtures. J Chem Thermodyn. 2021;163:106596.
[26] Stanley HE. Introduction to phase transitions and critical phenomena. New York (NY): Oxford University Press; 1971.
[27] Anisimov MA. Critical phenomena in liquids and liquid crystals. Philadelphia (PA): Gordon and Breach; 1991.
[28] Bagnuls C, Bervillier C. Nonasymptotic critical behavior from field theory at D = 3 - the ordered phase. Phys Rev B. 1985;32:7209–7231.
[29] Bagnuls C, Bervillier C, Meiron DI, et al. Nonasymptotic critical behavior from field theory at D = 3.2- the disordered phase. Phys Rev B. 1987;35:3585–3607.
[30] Zinn-Justin J. Precise determination of critical exponents and equation of state by field theory methods. Phys Rep. 2001;344:159–178.
[31] Ema K, Nounesis G, Garland CW, et al. Calorimetric study of smectic polymorphism in octyloxy phenyl-nitrobenzoyloxy benzoate + decyloxyphenyl-nitrobenzoyloxy benzoate mixtures. Phys Rev A. 1989;39:2599–2608.
[32] Chen X, Clark NA. Bull Am Phys Soc. 2022;67. (submitted).
[33] Fisher ME, Sarbach S. Nonuniversality of tricritical behavior. Phys Rev Lett. 1978;41:1127–1130.
[34] Sarbach S, Fisher ME. Tricritical coexistence in 3 dimensions: multicomponent limit. Phys Rev B. 1979;20:2797–2817.
[35] Stephen MJ. Universality and tricritical points in 3 dimensions. J Phys C. 1980;13:L83–L86.
[36] Stine KJ, Garland CW. Calorimetric study of nematic to smectic-A tricritical behavior. Phys Rev A. 1989;39:3148–3156.
[37] Ema K, Tagaki A, Yao H. Gaussian tricritical behavior of the heat capacity at the smectic-A-smectic-C liquid crystal transition. Phys Rev A. 1996;53:R3036–R3039.
[38] Stauffer D, Ferrer M, Wortis M. Universality of second-order phase transitions – scale factor for correlation length. Phys Rev Lett. 1972;29:345–348.